PAPER

Effect of microstructure on the nanotube growth by anodic oxidation on Ti-10Nb alloy

To cite this article: A R Luz *et al* 2017 *Mater. Res. Express* **4** 076408

Materials Research Express

PAPER

RECEIVED
30 March 2017

REVISED
28 June 2017

ACCEPTED FOR PUBLICATION
3 July 2017

PUBLISHED
27 July 2017

Effect of microstructure on the nanotube growth by anodic oxidation on Ti-10Nb alloy

A R Luz[1], C M Lepienski[1], S L Henke[2], C R Grandini[3] and N K Kuromoto[1,4]

[1] Programa de Pós-Graduação em Engenharia e Ciência dos Materiais—PIPE, Universidade Federal do Paraná, 81531-990 Curitiba—PR, Brazil
[2] Departamento de Engenharia Mecânica, Universidade Federal do Paraná, 81531-990 Curitiba—PR, Brazil
[3] Departamento de Física, Universidade Estadual Paulista, campus de Bauru, 17033-360 Bauru—SP, Brazil
[4] Departamento de Física, Universidade Federal do Paraná, 81531-990 Curitiba—PR, Brazil

E-mail: arossettoluz@gmail.com

Keywords: Ti-10Nb alloy, microstructure, nanotubes, nanostructured walls, Raman mapping

Abstract

Several papers have reported the grown self-organized nanotube arrays on pure Ti and its alloys to improve the surface of these materials for biomedical applications. The growth of nanotubes can be influenced by microstructure of material; however, few papers concerning this topic have been published. The aim of this work was to investigate the morphology, the cross-section view and the oxides in nanotube arrays in relationship to the microstructure of the Ti-10Nb alloy. The growth of nanotubes on the Ti-10Nb alloy obtained by anodic oxidation (AO). The Ti-10Nb alloy is composed by alfa and beta phases that were investigated by metallographic analysis, patterns of x-ray diffraction and EDS analysis. SEM images and EDS analysis revealed the morphology was composed by self-organized nanotube arrays on the alpha phase and walls with transversal holes on beta phase. X-ray patterns show crystalline oxides formation. Raman spectrum confirms the presence of anatase and Nb_2O_5 oxides. A significant contribution of the Nb_2O_5 was observed by bi-dimensional (x, y) Raman mapping, which also showed that the all oxide film was homogeneous oxide distributed on Ti-10Nb alloy. The nanostructured films have higher thickness in the beta than in the alpha phase, and have a small different in structure and oxide composition; as observed by SEM and Raman mapping. The results indicate that the microstructure of the Ti-10Nb affects the nanotubes morphology and the cross-section view, but the oxide formation was similar for all regions analyzed.

1. Introduction

Titanium (Ti) and Ti-6Al-4V alloy are widely used as biomaterial due to excellent mechanical properties, biocompatibility and corrosion resistance [1, 2]. However, researchers reported possible adverse effects Ti-6Al-4V alloy. Vanadium (V) can be accumulated in some parts of the body, such as bone, liver, and kidney. The presence of V ions in human tissues can change the kinetics of enzymatic activity associated with the inflammatory response of the cells. Aluminum (Al) increases the potential for the development of Alzheimer's disease [3]. As an alternative of the Ti-6Al-4V alloy, new β-type Ti alloys containing non-toxic elements (Nb, Zr, Ta, Mo, Sn) have been proposed for biomedical applications. In general, β-type Ti alloys have the best combination of the properties: low elastic modulus, corrosion resistance in body fluids, no allergic, and excellent biocompatibility [3].

Ti and its alloys are bioinert materials, so the surface modifications can be employed to making them bioactive [1, 2]. Nanotube arrays can be grown on their surfaces by anodic oxidation (AO) process [4–10]. These structures can enhance bone cell growth and improve the osseointegration process due to the chemical bond between bone and implant; avoiding that occur the bone resorption and eventual failure of the implant [5]. Besides that, due to oxide layer, as TiO_2, the nanotube arrays show better corrosion resistance than flat metallic biomaterials [5].

The morphology of nanotube arrays on the pure Ti or monophasic alloys is self-organized over all surface [4]. For pure Ti was reported the growth of nanotubes and quality of oxide depend on crystallographic plane orientation and interstitial solution [11–14].

The nanotubes morphology grown on Ti alloys may depend on the microstructure of material [10, 15]. However, few researchers explain about this subject [16]. The morphology of nanotubes growth on biphasic alloys was affected by the microstructure [15–18], while other researchers were not observe this behavior [19, 20]. For example, Jang *et al* [20] grown nanotubes with 1M H_3PO_4 + 0.8 wt.% NaF electrolyte on monophasic alloys (Ti-10Nb and Ti-40Nb) and biphasic alloys (Ti-20Nb and Ti-30Nb), they observed that the nanotubes morphologies were not affected by the microstructure of alloys and related the size diameters of tube with of amount Nb in Ti-*x*Nb alloys. Despite the nanotubes morphology influenced by the microstructure of substrate [15–18], details of the growth on different phases and the features of the cross-section view were not published yet.

The Raman scattering is widely used to investigate the oxide composition of nanotubes, since the bands Raman to titanium oxides are well knew [12, 21–23]. Measurements were done on different Ti grains after anodization by Leonardi *et al* [12]. They used the punctual Micro-Raman scattering to investigate the structure and phase composition of nanotubes grown on pure Ti. The results showed a disordered titanium oxide structure, which was attributed to disordered grain boundaries or amorphous oxide matrix [12].

The Raman mapping allows to analyze the homogeneity of the sample, and the depth profile can also be obtained [21]. By the way, this technique has been widely used to study the properties of twisted bilayer graphene [20] and carbon nanotubes [21]. However, to the best of our knowledge, this technique was not used for investigate the homogeneity of nanotube arrays. Therefore, it was proposed to employ this technique to investigate the oxide composition of nanostructure film grown on the Ti-10Nb biphasic alloy, qualitatively. Raman mapping was used to investigate the homogeneity of nanostructured film by bi-dimensional (x, y) Raman mapping, and the thickness by depth scan Raman mapping.

The present communication investigated the effect of microstructure on nanotube growth by AO on the Ti-10Nb biphasic alloy. The focus was to analyze the morphology at the different steps of the anodic process to obtain the nanostructured film, thickness and the oxide composition of anodic film.

2. Materials and methods

The raw materials used to manufacture the alloy were commercially pure titanium grade 2 (cp-Ti) with 99.7% purity and niobium (Nb) with 99.8% purity. For melting of these metals, it was used an arc-melting furnace with copper crucible water cooled, non-consumable tungsten electrode, and an argon-controlled atmosphere. The raw materials were melted by electric arc for five times to guarantee homogeneity. The alloy cooling was done in the furnace at a rate of 5 °C min^{-1}. After that, the samples were submitted to heat treatment (1000 °C/24 h) in an ultra-vacuum furnace to relieve the residual stress resulted by melting process. The ingots with 10% wt. of Nb were obtained after melting process, which were submitted again at the same heat treatment to recrystallize the microstructure of the material modified by forging. From the ingots, samples were obtained with 9 mm diameter and 2 mm thickness.

For the microstructural analysis, the samples were sanded with sandpaper (220–1200) and polished with alumina (1 μm). The samples were then etched with a Kroll solution consisting of 1.5 ml HF + 4 ml HNO_3 + 94 ml H_2O. The microstructures were analyzed by optical microscopy (FV10i—Olympus).

The Ti-10Nb alloy phases were determined by x-ray diffraction (Bruker—D8 Advance diffractometer with LYNXEYE-XE detector), operating at 40 kV and 20 mA, Cu K α radiation, in Bragg-Brentano geometry (2θ − 20° to 80°) in step scan of 2° min^{-1}.

In addition the microstructure, chemical composition and distribution of elements in polished Ti-10Nb alloy were analyzed by scanning electron microscopy (SEM—FEI Quanta 450 FEG) and energy dispersive spectroscopy (EDS) in line mode.

The elastic modulus of grade 2 Ti and Ti-10Nb alloy were obtained by instrumented indentation technique (MTS NanoIndenter XP). Berkovich-type diamond tip and loads up to 500 mN were used. The values were calculated following the Oliver–Pharr method [24]. Sets of 25 indentations were performed on each sample.

Prior to the anodization, the Ti-10Nb samples were abraded with sandpapers (220–1200) and the finally polished with SiO_2 colloidal suspension of 0.05 mm. The samples were ultrasonically cleaned in acetone, isopropyl alcohol, and deionized water, for 15 min each bath and dried at 40 °C for 24 h in an incubator.

The AO was carried out with a conventional two-electrode configuration with platinum as a counter electrode and the Ti-10Nb alloy as the working electrode. The nanotubes were obtained using 1.0 M 0.5 M Na_2SO_4 + 0.1%wt HF electrolyte. The applied potential was 20 V under potentiostatic mode, at room temperature. It was used three different anodization times, which correspond to the three stages of the nanofilm growth. In the third condition it was used the anodization time of 40 min. Current profiles as a function of oxidation time were obtained by Excel program.

The morphology and cross-sectional view of nanotube arrays were obtained by SEM (FEI Quanta 450 FEG). The software Image J was used to measure the thickness of the film. The cross-sectional thickness measurements were carried out directly on the mechanically cracked sample.

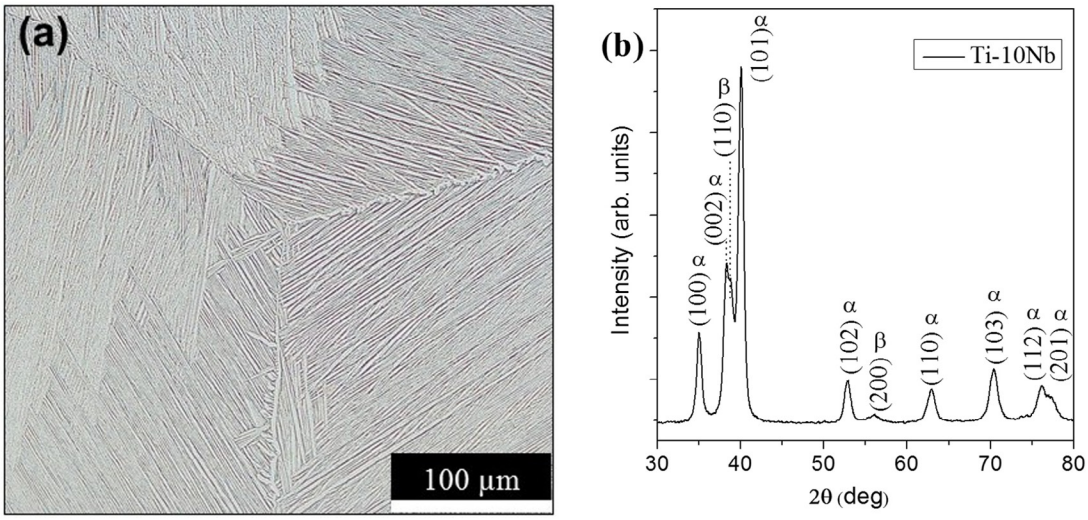

Figure 1. Structural analysis of the Ti-10Nb alloy (a) optical microscopy, (b) x-ray diffraction.

EDS analysis was done after the anodic process to investigate the relationship between the nanostructured morphology and the microstructure of the Ti-10Nb alloy.

The x-ray diffraction equipment (Bruker—D8 Advance, LYNXEYE-XE detector) was used to identify the phases of oxide formed at the three stages of the growth of film during the anodic process. Due to presence of the thin film the grazing x-ray incidence was employed at $\theta = 3°$, divergence slit of 1.0 mm and 1.56% nickel filter was used to cut the k_β radiation, at 40 kV and 20 mA, Cu K α radiation.

The Witec alpha 300R confocal Raman system was used to obtain the Raman spectra, surface and thickness mappings of nanostructured film. The laser used was He–Ne at 532 nm, spot size ~2 μm, laser power of 36 mW, with integration of 10 accumulations and acquisition time of 1 s. The Raman spectra were done of the polished Ti-10Nb alloy and of steps of the growth of nanostructured film. The bi-dimensional (x, y) Raman mapping was done to analyze the distribution of oxides into the surface of the Ti-10Nb alloy anodized. While the depth scan Raman mapping was done to analyze the distribution of oxides inside the film, i.e. the distribution of the oxide into the thickness of nanostructured film. The Raman mappings were acquired by a 50× objective using the same configuration of the Raman spectra. The bi-dimensional (x, y) Raman mapping was obtained from 150 point/line and an (25×25) μm area. The depth scan Raman mapping was obtained from scan width 25 μm, depth scan of 20 μm, 50 point/line and 50 layer/scan. Each scan corresponds to different laser focus depth. The data of Raman mappings were analyzed with the sum method by Witec Project software.

3. Results and discussions

3.1. Microstructural analysis

The optical micrograph (figure 1(a)) shows the microstructure of the Ti-10Nb alloy, which was composed of mainly $\alpha + \beta$ colonies. It also observed a lamellar structure and needle-like structure [25]. Figure 1(b) shows the peaks on the XRD patterns of the homogenized Ti-10Nb alloy, which was composed by $\alpha + \beta$ phases. The presence of peaks of the β phase shows that the Nb element in Ti-Nb system plays the role as a stabilizer of β phase [26]. When Ti is alloyed with a lower content of Nb the α phases dominate in alloy [27], as observed in the figure 1(b).

Figure 2 shows the SEM image of the Ti-10Nb alloy. It is a typical lamellar structure that is characteristic of alloys compound by $(\alpha + \beta)$ phases [3, 25], as per figures 1 and 2. The insert in figure 2 corresponds to the EDS obtained in line mode that was done to investigate the chemical composition of the Ti-10Nb alloy. The dot line region in the figure 2 indicated the analyzed region. The light gray regions present higher Nb concentration than dark gray regions. Unlike, Ti concentration decreases in the light gray regions and increase in the dark gray regions. Moreover, when the lamellar structure was wide, the EDS line was also wide; while to the narrow light regions was observed a narrow EDS line too. Therefore, the dark regions are rich in α-phase and the light regions are rich in β-phase, since the Nb is a beta stabilizer element [3, 25]. Furthermore, the overall concentration of the Ti and Nb were around of the expected, 90 wt.% for Ti and 10 wt.% for Nb. Therefore, the Ti-10Nb alloy was well homogenized since Nb clusters in the alloy were not observed.

The elastic modulus values obtained by instrumented indentation were (131 ± 4) GPa for grade 2 Ti and (110 ± 2) GPa for Ti-10Nb alloy. This decrease in the elastic modulus is due to the presence of the β phase and

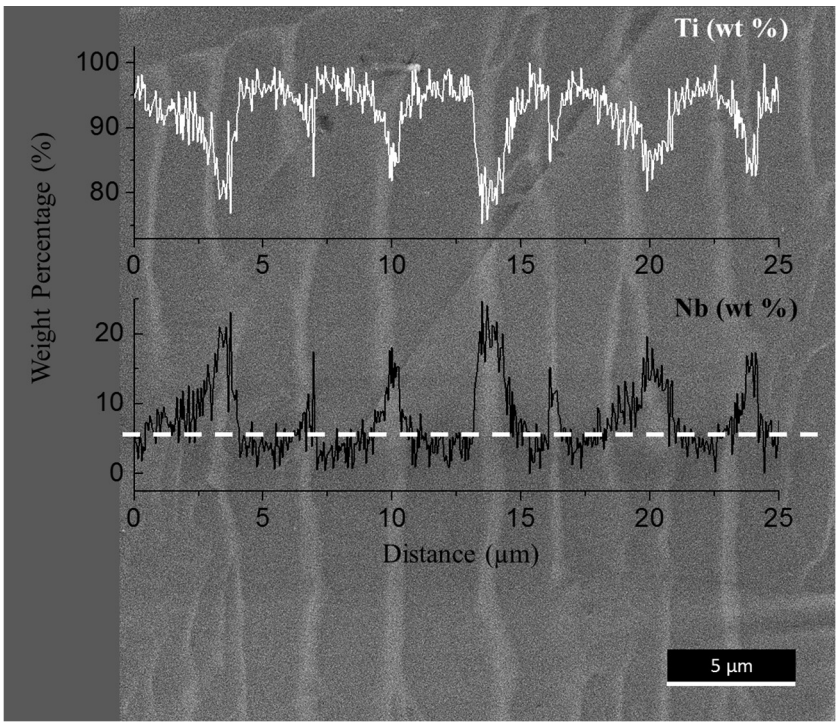

Figure 2. SEM image of the polished Ti-10Nb alloy. The insert is the EDS counts for Nb and Ti in line mode, measured at the white dot line region. The black line correspond to Nb and the white line to Ti (in wt.%).

can reduce the stress shielding effect that is responsible for bone resorption, loosening, and eventually replacement surgeries [28, 29].

3.2. Nanotubes morphology and cross-section view

Figure 3 shows the typical current versus time curve during nanotubes growth [7–9] on the Ti-10Nb alloy surface. The regions I, II and III are the stages of the nanotubes growth process, which correspond to SEM imagens in the figures 4(a)–(c), respectively.

The region I (figure 3) corresponds to a process with a quick current decrease due to a homogeneous compact oxide formation [7–9] on the Ti-10Nb surface, as can see it in the figure 4(a).

The current in the region II (figure 3) starts to increase, and then reaches a maximum, indicating the beginning of nucleation of irregular nanopores in the compact oxide formed previously. However, the nanopores formation depends on microstructure of the Ti-10Nb alloy (figure 4(b)). So that, when start the nanopores formation due the presence of the fluorine ions in the electrolyte [7–9]; the microstructure of the Ti-10Nb alloy was revealed (compare the figures 2 and 4(b)). The enlarged square in the figure 4(b) shows that on the β phase the pores were much smaller than on the α phase, indicating a preferential dissolution of oxide formed on alpha phase. Probable it is due to a different oxide composition grown on different phases.

The different pores can interfering with each other, and can occurs a competition by the available current [10], so it was observed the small oscillations at the stage III. The current reaches a stable plateau (region III—figure 3), indicating that there is an equilibrium between the oxidation and dissolution process by fluorine ions; and consequently occurs the formation of nanostructured film (figures 4(c) and (d)) [7–9].

The nanotubes growth process is well known [4–10]. As a rule, during the anodization occurs, simultaneously, the continual oxide growth at the inner interface and the chemical dissolution of oxide [10]. Nanotube arrays grown on biphasic alloys can show non-uniform morphology because occurs a selective dissolution of less stable elements and different reaction rates on different phases of an alloy [4, 9, 10, 30].

Figures 4(c) and (d) show a self-organized nanotube arrays with random diameters grew on the regions rich in α-phase, as obtained to pure Ti or monophasic alloys [7–9]. The regions rich in β-phase showed a lamellar structure and the formed oxide shows different structure and morphology. Different morphologies were also observed in reports for nanotubes grown on biphasic ($\alpha + \beta$) alloys [15–18].

The points in figure 4(d) correspond to EDS analysis regions. The table 1 shows that 1–3 points had the Nb content higher than 4–6 points. Unlike, the Ti content was lower to the 1–3 points than 4–6 points. In agreement with figure 2 and EDS analysis reported by Jang *et al* [20] to Ti-xNb (x = 10–40 wt.%).

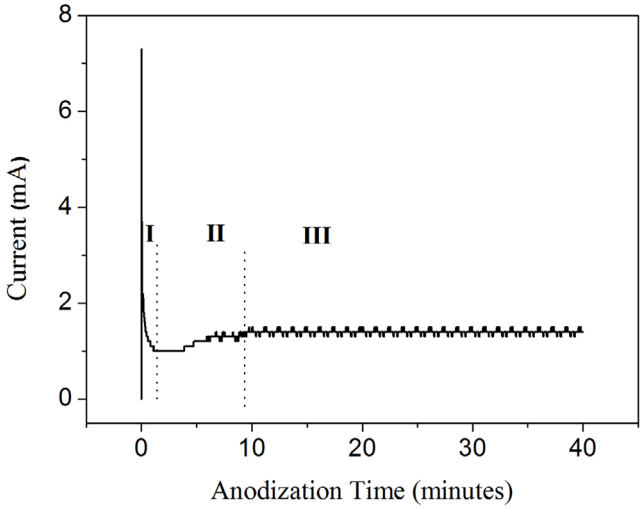

Figure 3. Current-time anodizing curve to Ti-10Nb alloy: I, II and III are the different nanotubes growth process steps.

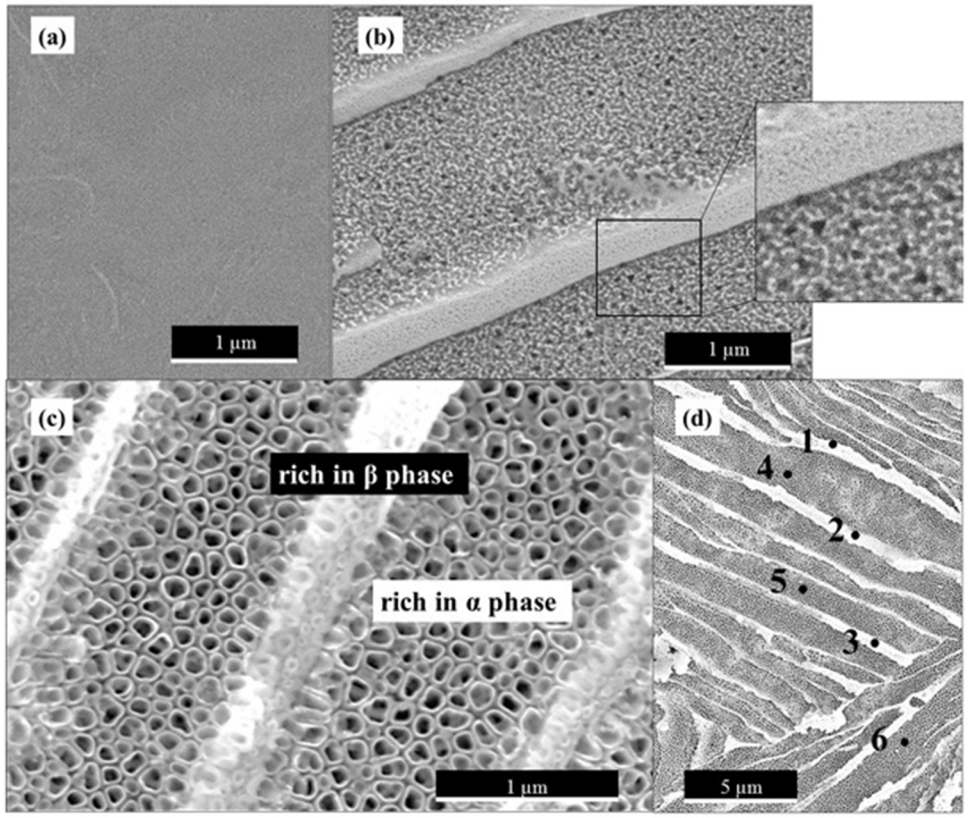

Figure 4. Morphology of the Ti-10Nb alloy anodized at 20 V in 1 M Na_2SO_4 as a function of anodization time, related to the stages of anodic process in the figure 3: (a) stage I, (b) stage II, with an enlarged insert, (c) and (d) stage III at different magnifications. The points in the (d) are corresponding to EDS analysis (table 1).

In order to investigate the different morphologies of oxides on α and β phase the cross-section of the oxide layers were detailed investigate, as shown in figure 5. In the region rich in α phase grew a self-organized nanotube arrays were average length about 0.59 μm. and a lamellar structure grew in the region rich in β phase, likewise as observed in figures 4(c) and (d).

In the beta phase region, due to the presence of higher Nb concentration, nanotubes were not formed in the same way. The oxide walls observed in figure 5 on β phase were significantly less attacked than oxide on the α phase region. This process results in an oxide layer on the β phase that is 1.36 μm higher than oxide nanotubes grown on α phase. Differently from oxide on alpha phase, these oxide walls on β phase are subjected to an attack by the fluorine ions in the transverse direction of the walls forming nanotubes perpendicular to the existing nanotubes in the α phase.

Table 1. EDS analysis of anodic film on the Ti-10Nb alloy.

Phase	Point	Ti (wt.%)	Nb (wt.%)	O (wt.%)	F (wt.%)
β	1	54.76 ± 0.25	11.04 ± 0.09	30.83 ± 0.29	3.36 ± 0.16
	2	48.59 ± 0.22	9.47 ± 0.08	37.49 ± 0.26	4.45 ± 0.17
	3	52.05 ± 0.23	9.96 ± 0.08	33.82 ± 0.27	4.17 ± 0.16
α	4	66.03 ± 0.29	5.37 ± 0.07	25.74 ± 0.30	2.87 ± 0.14
	5	72.85 ± 0.31	6.03 ± 0.32	19.28 ± 0.32	1.85 ± 0.13
	6	65.56 ± 0.29	6.24 ± 0.07	25.66 ± 0.30	2.54 ± 0.14

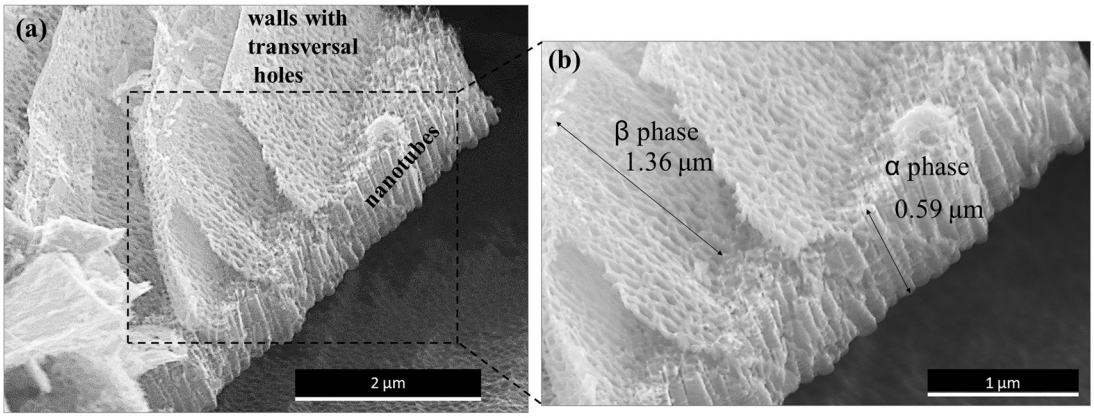

Figure 5. Cross-sectional view at different magnifications of oxide film morphology on the Ti-10Nb alloy: nanotubes on α phase and walls with transversal holes on β phase.

Table 1 shows that the fluorine in the electrolyte was incorporated in the film [6]. The presence of oxygen is expected due to oxide formation [6]. The EDS measurement concentration of oxygen and fluorine in the regions rich in β phase was higher than in regions rich in α phase.

The oxides formed in each one of the phases have different concentrations of Nb. The attack of the fluorine ions on the oxides in the alpha phase is different from the attack on the oxides in the beta phase. Probably due to different oxide composition, the oxidation in the beta phase is less attacked, forming a wall ~1.36 μm above the nanotubes of the alpha phase oxides.

The oxide walls on the beta phase are attacked transversely forming 'nanotubes-like pores', which results in a wall with transverse holes.

All results (figures 1–5 and Table 1) showed the α and β phases influence the nanotube formation on the Ti-10Nb alloy. Although of non-uniform morphology (figure 5), it is suitable for biomedical applications, as shown on Ti-*x*Zr that presented a good performance to cell tests [17].

3.4. Oxides phases

Figure 6 shows the peaks on the XRD patterns of the Ti-10Nb alloy in comparing to the stages of the anodic process (figure 3). The significant change were the peaks at 26°, 37° and 41°. There are no significant differences between the x-ray spectra for the different oxidation times (stages I–III). The peaks at 26° and 37° correspond to the anatase phase. Although the peak at 41° be well defined in all spectra, it was not possible to index this peak with stoichiometric oxides of Nb or Ti. It is possible to correspond to non-stoichiometric oxides of Ti and/or Nb, with fluorine ions incorporation, as observed in the composition of the film indicated in table 1.

The literature shows that most nanotubes obtained by AO process are amorphous. However, several authors showed crystalline nanotubes without any annealing, due to the oxide formation in the oxide-metal interface [6,10]. Our results indicated that crystalline regions are present, as observed in figure 6.

Figure 7 shows Raman spectra for the polished Ti-10Nb alloy and for different oxidation times (figure 3 stages I–III).

The information about lattice vibration frequencies of a crystal can be obtained by measurement of the Raman spectrum [31]. The Raman's effect can occurs due to the interaction of the incident light of angular frequency with the crystal [31]. This interaction can create or destroy one or more lattice vibration quanta (phonons), and then the energy obtained or lost by the lattice is compensated by an increase or decrease in the frequency of the scattered light [31]. The maximum wavenumber of the majority of crystals have lattice vibrations that varies between 100 cm^{-1} and 1000 cm^{-1} or higher [31]. the wavenumber for titanium and niobium oxides are inside in this range, as shown by several researchers [12, 21–23, 32].

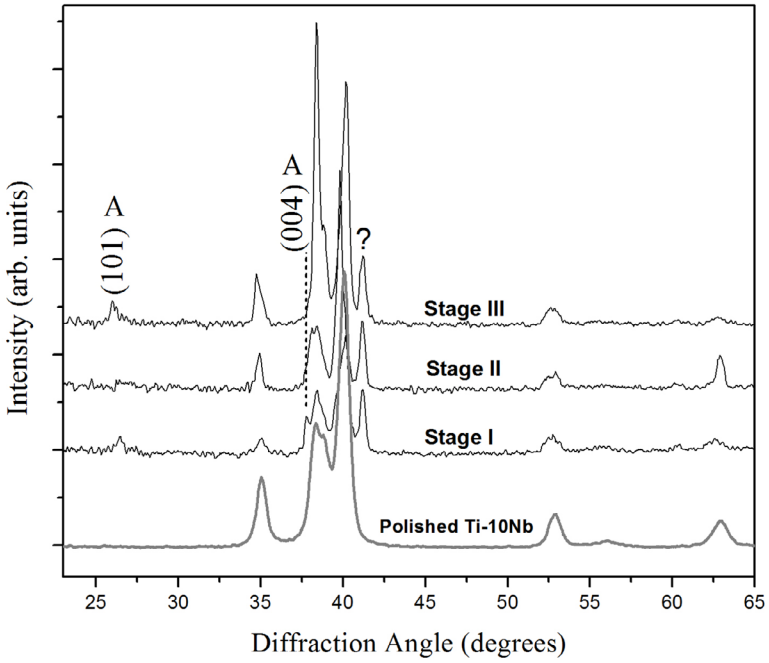

Figure 6. X-ray diffraction spectra: polished Ti-10Nb and for different oxidation times (figure 3 stages I–III). '***A***' correspond to anatase peaks.

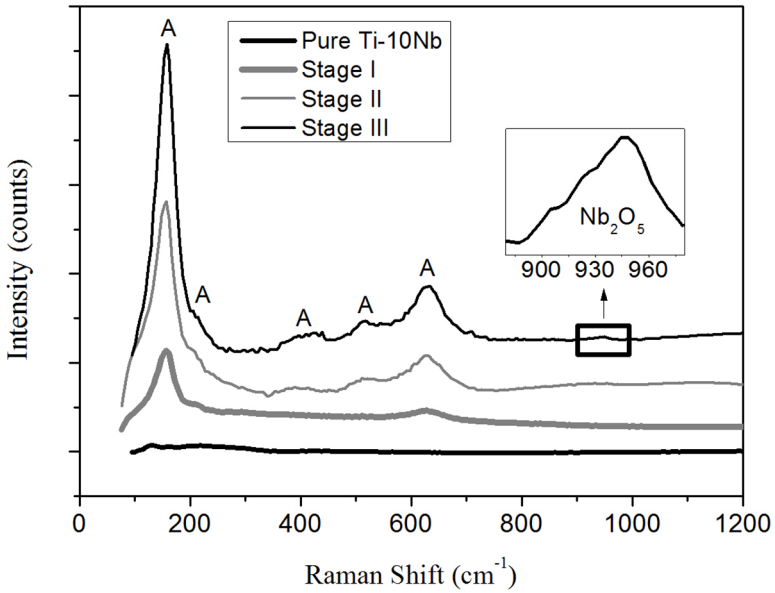

Figure 7. Raman spectra: polished Ti-10Nb and for different oxidation times (stages I–III). '***A***' correspond to anatase peaks.

As expected the signal Raman to polished Ti-10 Nb alloy present no peaks, since the primitive oxide on alloy is very thin [2]. The stage I of the anodic process (figure 3) shows anatase peaks (156.5 cm^{-1}, 210.30 cm^{-1} and 630.44 cm^{-1}) [23], indicating that compact oxide film grew on Ti-10Nb alloy (figure 4(a)).

In stages II and III are observed peaks in 400 cm^{-1} and 510 cm^{-1} [23], corresponding to the anatase phase. The peak at 950 cm^{-1} observed in stage III corresponds to Nb_2O_5 [32].

The oxides of nanotubes growth on Ti alloys may have mixtures of oxides of elements that compound the alloy [6]. Semboshi *et al* [33] reported to anodic oxides grown on Nb-*x*Ti (x = 1–15 wt.%) the niobium oxide formation depend on the amount of Nb there is in the alloy, and the formation rate of titanium oxide is faster than niobium oxide [16, 20]. Therefore, a major contribution of the TiO_2 was expected. In view of the content of Ti is higher than Nb in the Ti-10Nb alloy.

Bi-dimensional (x, y) Raman mapping is shown in figure 8. The figure 8(a) is the area correspond to contribution of the all spectrum of the stage III (figure 7), and Raman images for peak intensities: 950 cm^{-1} (b): 120–230 cm^{-1} (c), 400 cm^{-1} (d), 510 cm^{-1} (e), 630 cm^{-1} (f). The Raman mapping (figure 8(a)) shows an almost

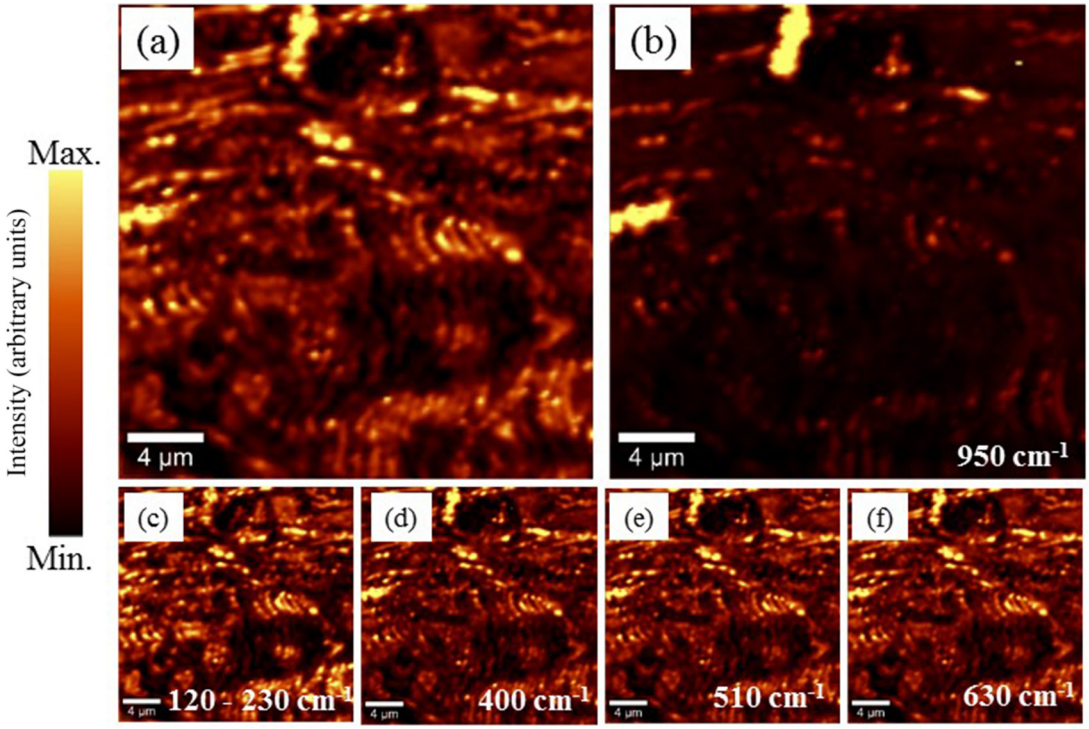

Figure 8. Bi-dimensional (x, y) Raman mapping of the Ti-10Nb alloy anodized (a). Raman images for peak intensities: 950 cm^{-1} (b), 120–230 cm^{-1} (c), 400 cm^{-1} (d), 510 cm^{-1} (e) and 630 cm^{-1} (f).

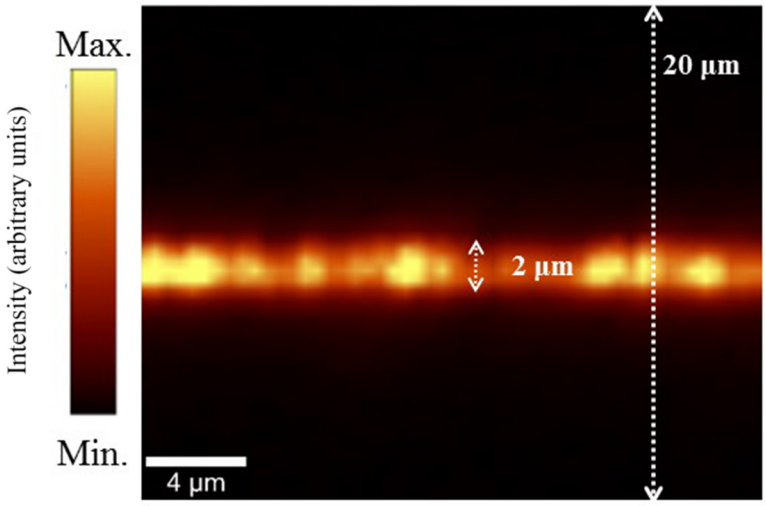

Figure 9. Depth scan Raman mapping of the Ti-10Nb alloy anodized.

homogeneous oxide distribution, once the morphology depends on the microstructure of the Ti-10Nb substrate (figures 4 and 5).

The spectrum obtained for the stage III (figure 7) is characteristic of the anatase phase; in conformity the x-ray pattern that shown a significant contribution of the anatase. In this way the similar feature in the figures 8(c)–(f) can be attributed to the presence of anatase.

However, the lights regions in figure 8(b) can be attributed to presence of the Nb_2O_5 since this image depends on this contribution. At the band around 950 cm^{-1} just correspond to Nb_2O_5, while of the other bands (200–630 cm^{-1}) can have overlap of titanium and niobium oxides [23, 32]. Thus, the lighters regions in figures 8(c)–(f) correspond to Nb_2O_5 contribution.

Figure 9 shows the depth scan Raman mapping of the Ti-10Nb alloy anodized, which correspond to contribution of the all spectrum of the stage III (figure 7). A significant relationship was observed between the film thickness obtained by SEM (figure 5) and the signal intensity of the depth scan Raman mapping (figure 9), since the order of magnitude is close to 2 μm for the both results. The measurement of the figure 9(a) was done with depth

scan of 20 μm, so, the 9 μm above and under the light region in figure 9(a) are the air and the Ti-10Nb substrate, respectively. Therefore, the light region (figure 9(a)) corresponds to the nanostructured film grown by anodic process.

Nanotubes composed of oxides mixtures, such as TiO_2, Nb_2O_5, SnO_2, and ZrO_2 have the same biological behavior that titanium oxides [6], that is known in the biomaterials area they are non-toxic, biocompatible, and corrosion resistant [4].

The successful Raman mapping depends on the quality of sample, since for large sample with irregular shape or heterogeneous structure this analysis is very difficult [34]. The film grew on the Ti-10Nb was adequate structure for the Raman mappings measurements. Our data of the Raman mappings were consistent, considering all analysis done (figures 1–9). Therefore, we demonstrated that the Raman mapping is a powerful technique for investigate nanostructure films obtained by anodic process.

4. Conclusions

Metallographic analysis and x-ray diffraction showed that the Ti-10Nb alloy is composed of α and β phases. A self-organized nanotube structure grew on rich α phase regions, with random diameters and length 0.59 μm. A lamellar oxide structure grew on rich β phase regions, forming a wall ~1.36 μm above the nanotubes of the α phase oxides. The fluorine ions attack preferentially the oxide on α phase, as reveled by its lower thickness compared to oxide grown on β phase. In addition, the lamellar walls oxide structure on β phase is subjected to fluorine ions as indicated by formation of transversal holes in lamellar walls. X-ray patterns shows crystalline oxides formation. Raman spectrum confirms the presence of anatase and Nb_2O_5 oxides. Raman surface mapping shows that the Nb_2O_5 is distributed in some points, probably in in beta phase regions. The thickness of the oxide layer was about 2 μm, according to SEM and Raman thickness analysis.

Acknowledgments

The authors thank the Electron Microscopy Center of UFPR and the X-ray Optics Laboratory of the Department of Physics UFPR for the facilities, the Araucaria Foundation and CAPES for financial support.

ORCID

C M Lepienski https://orcid.org/0000-0002-9759-9704
C R Grandini https://orcid.org/0000-0002-3336-309X

References

[1] Ratner B D and Bryant S J 2004 Biomaterials: where we have been and where we are going *Annu. Rev. Biomed. Eng.* **6** 41–75
[2] Liu X, Chu P and Ding C 2004 Surface modification of titanium, titanium alloys, and related materials for biomedical applications *Mater. Sci. Eng.* R **47** 49–121
[3] Niinomi M 2003 Recent research and development in titanium alloys for biomedical applications and healthcare goods *Sci. Technol. Adv. Mater.* **4** 445–54
[4] Roy P, Berger S and Schmuki P 2011 TiO_2 nanotubes: synthesis and applications *Angew. Chem., Int. Ed. Engl.* **50** 2904–39
[5] Ghicov A and Schmuki P 2009 Self-ordering electrochemistry: a review on growth and functionality of TiO_2 nanotubes and other self-aligned MO(x) structures *Chem. Commun.* **5** 2791–808
[6] Khudhair D, Bhatti A, Li Y, Hamedani H A, Garmestani H, Hodgson P and Nahavandi S 2016 Anodization parameters influencing the morphology and electrical properties of TiO_2 nanotubes for living cell interfacing and investigations *Mater. Sci. Eng.* C **59** 1125–42
[7] Indira K, Mudali U K, Nishimura T and Rajendran N 2015 A review on TiO_2 nanotubes: influence of anodization parameters, formation mechanism, properties, corrosion behavior, and biomedical applications *J. Bio- Tribo- Corros.* **1** 28
[8] Kulkarni M, Mazare A, Gongadze E, Perutkova S, Kralj-Iglic V, Milosev I, Schmuki P, Iglic A and Mozetic M 2015 Titanium nanostructures for biomedical applications *Nanotechnology* **26** 62002
[9] Minagar S, Berndt C C, Wang J, Ivanova E and Wen C 2012 A review of the application of anodization for the fabrication of nanotubes on metal implant surfaces *Acta Biomater.* **8** 2875–88
[10] Macak J M, Tsuchiya H, Ghicov A, Yasuda K, Hahn R, Bauer S and Schmuki P 2007 TiO_2 nanotubes: self-organized electrochemical formation, properties and applications *Curr. Opin. Solid State Mater. Sci.* **11** 3–18
[11] Crawford G A and Chawla N 2009 Tailoring TiO_2 nanotube growth during anodic oxidation by crystallographic orientation of Ti *Scr. Mater.* **60** 874–7
[12] Leonardi S, Bassi A L, Russo V, Di Fonzo F, Paschos O, Murray T M, Efstathiadis H, Agnoli A and Kunze J 2012 TiO_2 nanotubes: interdependence of substrate grain orientation and growth characteristics *J. Phys. Chem.* **116** 384–92
[13] Macak J M, Jarosova M, Jäger A, Sopha H and Klementová M 2016 Influence of the Ti microstructure on anodic self-organized TiO_2 nanotube layers produced in ethylene glycol electrolytes *Appl. Surf. Sci.* **371** 607–12
[14] Leonardi S, Russo V, Li Bassi A, Di Fonzo F, Murray T M, Efstathiadis H, Agnoli A and Kunze-Liebhäuser J 2014 TiO_2 nanotubes: interdependence of substrate grain orientation and growth rate *ACS Appl. Mater. Interfaces* **7** 1662–8
[15] Kim W G, Choe H-C, Ko Y-M and Brantley W A 2009 Nanotube morphology changes for Ti–Zr alloys as Zr content increases *Thin Solid Films* **517** 5033–7

[16] Ferreira C P, Gonçalves M C, Caram R, Bertazzoli R and Rodrigues C A 2013 Effects of substrate microstructure on the formation of oriented oxide nanotube arrays on Ti and Ti alloys *Appl. Surf. Sci.* **285** 226–34
[17] Choe H C 2011 Nanotubular surface and morphology of Ti-binary and Ti-ternary alloys for biocompatibility *Thin Solid Films* **519** 4652–7
[18] Ossowska A, Sobieszczyk S, Supernak M and Zielinski A 2014 Morphology and properties of nanotubular oxide layer on the 'Ti–13Zr–13Nb' alloy *Surf. Coat. Technol.* **258** 1239–48
[19] Kim E S, Jeong Y H, Choe H C and Brantley W A 2013 Formation of titanium dioxide nanotubes on Ti–30Nb–*x*Ta alloys by anodizing *Thin Solid Films* **549** 141–6
[20] Jang S H, Choe H C, Ko Y M and Brantley W A 2009 Electrochemical characteristics of nanotubes formed on Ti–Nb alloys *Thin Solid Films* **517** 5038–43
[21] Mazzolini P, Russo V, Casari C S, Hitosugi T, Nakao S, Hasegawa T and Li Bassi A 2016 Vibrational-electrical properties relationship in donor-doped TiO_2 by Raman spectroscopy *J. Phys. Chem.* C **120** 18878–86
[22] Li Bassi A *et al* 2005 Raman spectroscopy characterization of titania nanoparticles produced by flame pyrolysis: the influence of size and stoichiometry *J. Appl. Phys.* **98** 074305
[23] Frank O, Zukalova M, Laskova B, Kürti J, Koltai J and Kavan L 2012 Raman spectra of titanium dioxide (anatase, rutile) with identified oxygen isotopes (16, 17, 18) *Phys. Chem. Chem. Phys.* **14** 14567–72
[24] Oliver W C and Pharr G M 1992 An improved technique for determining hardness and elastic modulus using load and displacement sensing indentation experiments *J. Mater. Res.* **7** 1564–83
[25] Froes F H 2015 *Titanium—Physical Metallurgy, Processing, and Applications* (Materials Park, OH: ASM International)
[26] Cordeiro J M and Barão V A R 2017 Is there scientific evidence favoring the substitution of commercially pure titanium with titanium alloys for the manufacture of dental implants? *Mater. Sci. Eng.* C **71** 1201–15
[27] Byeon I-S, Hwang I-J, Choe H-C and Brantley W A 2016 Electrochemically-coated hydroxyapatite films on nanotubular TiNb alloys prepared in solutions containing Ca, P, and Zn ions *Thin Solid Films* **620** 132–8
[28] Santos P F, Niinomi M, Cho K, Nakai M, Liu H, Ohtsu N, Hirano M, Ikeda M and Narushima T 2015 Microstructures, mechanical properties and cytotoxicity of low cost beta Ti–Mn alloys for biomedical applications *Acta Biomater.* **26** 366–76
[29] Niinomi M 2008 Mechanical biocompatibilities of titanium alloys for biomedical applications *J. Mech. Behav. Biomed. Mater.* **1** 30–42
[30] Konig U and Davepon B 2001 Microstructure of polycrystalline Ti and its microelectrochemical properties by means of electron-backscattering diffraction (EBSD) *Electrochim. Acta* **47** 149–60
[31] Loudon R 1964 The Raman effect in crystals *Adv. Phys.* 423–82 doi:10.1080/00018736400101051
[32] Huang B X, Wang K, Churchb J S and Li Y-S 1999 Characterization of oxides on niobium by raman and infrared spectroscopy *Electrochim. Acta* **44** 2571–7
[33] Semboshi S, Bando K, Ohtsu N, Shim Y and Konno T J 2008 Structural and dielectric properties of anodic oxide film on Nb–Ti alloy vol 516 pp 8613–9
[34] Tian Y, Wu P, Liu Q, Wu X and Hou X 2016 Mapping for total surface-enhanced Raman scattering to improve its quantification analysis *Talanta* **161** 151–6